

First-principles stabilization of an unconventional collinear magnetic ordering in distorted manganites

S. Picozzi

CNR-INFM, CASTI Regional Lab, I-67010 Coppito (L'Aquila), Italy

K. Yamauchi

ISIR-SANKEN, Osaka University, Mihogaoka 8-1, Ibaraki, Osaka 567-0047, Japan

G. Bihlmayer and S. Blügel

Institut für Festkörperforschung, Forschungszentrum Jülich, 52425 Jülich, Germany

(Dated: July 15, 2018)

Abstract

First-principles calculations have been performed for different collinear magnetic orderings in orthorhombic manganites, such as HoMnO_3 , TbMnO_3 and YMnO_3 , showing large GdFeO_3 -like distortions. Our results suggest that the AFM-E type ordering, experimentally observed in HoMnO_3 and recently proposed from model hamiltonian studies as a potentially novel phase, is indeed the magnetic ground state. Its stability is strongly connected with octahedral distortions and points to the relevance of *structural* more than *chemical* effects. The calculated exchange constants, extracted from a Heisenberg model used to fit the first-principles total energies, show that the ferromagnetic in-plane nearest-neighbour coupling is reduced compared to less-distorted manganites, such as LaMnO_3 . In parallel, the antiferromagnetic next-nearest-neighbour coupling along planar Mn-O-O-Mn paths in highly-distorted manganites plays a relevant role in the stabilization of the AFM-E spin configuration. In agreement with experiments, the density of states shows that this phase is insulating with an indirect band-gap of ~ 0.5 eV.

PACS numbers: 75.47.Lx, 75.30.Et, 71.70.-d

I. INTRODUCTION

Rare-earth manganites show a fascinating variety of physical phenomena,^{1,2} ranging from their unusual magneto-transport properties (leading to the well known colossal magnetoresistance²) to peculiar charge, spin and orbital orderings to recently discovered ferroelectricity^{3,4}. It is widely accepted that the intriguing manganites physics is intimately related to the profound interplay between the crystal lattice and the spin, charge and orbital degrees of freedom. In RMnO_3 with light rare-earth (R) cations (R= La, Pr, Nd) the collinear antiferromagnetic A-type (AFM-A) ordering (*i.e.* ferromagnetically (FM) coupled *ac* layers antiferromagnetically aligned along the *b* direction in the *Pnma* setting) is favored, whereas manganites toward the end of the series (R= Tb, Dy, Y) exhibit a sinusoidal magnetic structure defined by the propagation vector $(k_x, 0, 0)$. Recently, a new AFM phase has been observed in late-R HoMnO_3 ⁵ as well as in nickelates⁶, with an “up-up-down-down” spin ordering in the MnO_2 planes (the so called “E-type” in the Wollan-Koehler notation⁷), *i.e.* two Mn with up spins are alternated by two Mn with down spins along the principal axes of the in-plane cubic unit-cell, whereas the spins are reversed from plane to plane in the perpendicular direction. It is surprising that only very recently this phase has been proposed in undoped manganites^{8,9}, considered well-understood systems, where the E-type ordering was found to be stabilized in a wide region of the phase space.

The focus of the present work is therefore to compare our results with experimental observations suggesting AFM-E as the magnetic ground-state in HoMnO_3 and, more in general, to deeply investigate this non-conventional magnetic ordering, focusing in particular on the link between magnetic and structural properties. In closer detail, we consider different collinear magnetic alignments for three highly distorted manganites, HoMnO_3 , TbMnO_3 and YMnO_3 , in order to find the stable magnetic configuration and compare our results for the most studied LaMnO_3 . Surprisingly, we find that the AFM-E is the ground-state collinear phase for HoMnO_3 , TbMnO_3 and YMnO_3 and that its stabilization is mainly related to octahedral distortions that decrease the in-plane FM interaction between e_g states.

II. STRUCTURAL AND COMPUTATIONAL DETAILS

The simulations have been performed within the generalized gradient approximation (GGA) to the exchange–correlation potential in the density-functional framework. The all–electron full-potential linearized augmented plane-wave (FLAPW)¹⁰ formalism in the FLEUR¹¹ implementation has been used. Muffin-tin radii have been set to 2.5, 2.5, 2.5, 2.5, 2.0 and 1.5 a.u. for Tb, Y, La, Ho, Mn and O atoms, respectively, whereas the wave function cut-off was chosen as 3.8 a.u.^{−1}. Convergency was carried out using 24 special **k**-points in the orthorhombic Brillouin zone, whereas finer quantities (such as differences in the total energy) were checked using 192 special **k**-points.

In order to accurately treat within DFT the 4*f* electrons - that typically occupy an unphysical position slightly above the Fermi level (E_F) when considered as valence states - the Ho and Tb 4*f* electrons were kept in the core as an *open shell*¹² (with 7 and 1 (2) electrons in the up and down spin channel, respectively, for Tb (Ho)). An alternative solution to remove spurious effects related to the wrong energy position of Tb 4*f* electrons is to treat them as valence states using an LSDA+U approach.¹³ Tests performed on the undistorted perovskite-like cubic phase using LSDA+U¹⁴ on the 4*f* states showed that the resulting electronic structure is unchanged with respect to the “4*f*-in-core” treatment.

The unit cell in the GdFeO₃-like orthorhombic phase shows the *Pnma* symmetry (20 atoms/unit-cell, choosing *b* as the longest axis), with enormous distortions with respect to the ideal cubic perovskite (see Fig.1): due to the Jahn-Teller instability shown by the Mn³⁺ ion - with electronic configuration d^4 ($t_{2g}^3 e_g^1$) -, oxygen octahedrons are highly distorted and tilted (the average Mn-O-Mn angle is $\sim 145^\circ$, $\sim 142^\circ$ and $\sim 144^\circ$ for TbMnO₃, HoMnO₃ and YMnO₃, respectively, to be compared with the much larger value of $\sim 155^\circ$ in LaMnO₃). We recall that for YMnO₃ (and for other R smaller than Tb), the orthorhombic perovskite structure is no longer stable, the hexagonal non-perovskite structure competing in stability. However, the transition to the metastable orthorhombic *Pnma* can be obtained by high pressure synthesis¹⁵. The experimental lattice constants and internal positions according to neutron diffraction data - very similar for the three compounds, HoMnO₃, YMnO₃ and TbMnO₃ - have been used throughout the work¹⁵. In order to separate chemical and structural effects, we have also considered: a) LaMnO₃, having less distorted octahedrons and b) two “artificial” systems, namely *i*) YMnO₃ in the LaMnO₃ structure and *ii*) LaMnO₃ in the

YMnO₃ structure (denoted in the following as [YMnO₃]_{La} and [LaMnO₃]_Y, respectively).

III. RESULTS AND DISCUSSION

Let us first focus on YMnO₃, TbMnO₃, HoMnO₃ and LaMnO₃ in their equilibrium structure. In Table I we report the total energies (calculated per formula-unit containing one Mn atom) with respect to the FM phase. If we restrict to the FM and AFM - A, C and G orderings - (*i.e.* we neglect possible next-nearest-neighbors AFM coupling), the situation for HoMnO₃, TbMnO₃ and YMnO₃ is common to the well studied LaMnO₃, where the most stable magnetic configuration, as experimentally observed¹⁶ and theoretically confirmed^{17,18}, is the AFM-A type¹⁹. However, the inclusion of the AFM-E in the subset of considered magnetic configurations largely changes the scenario: interestingly, among the collinear magnetic orderings, *i)* HoMnO₃ show AFM-E as magnetic ground state, in excellent agreement with experiments, *ii)* both YMnO₃ and TbMnO₃ show the AFM-E type as stable configuration and *iii)* in LaMnO₃ the AFM-E is also not too high in energy compared to the AFM-A stable configuration. Indeed, this confirms what was proposed via model-hamiltonians, *i.e.* the occurrence of the AFM-E phase adjacent to the A-AFM in parameter space and competing with the FM metallic phase as well⁸. The differences between HoMnO₃, TbMnO₃ and YMnO₃ - having very similar structural parameters - suggests that, to some extent, the 4*f* moment affects the Mn ordering. In order to further highlight the effect of the spin-polarization due to the 4*f* Tb electrons, we considered a configuration in which these electrons are kept in the core, but they are equally shared between the majority and minority spins (4 in the up and 4 in the down channels, denoted as (4↑,4↓)), instead of the “normal” configuration - considered so far - in which there are 7 and 1 electrons in the up and down spin channels, respectively, denoted as (7↑,1↓)). The results show that the energy ordering of the different phases in TbMnO₃^(4↑,4↓) is very similar to YMnO₃, therefore suggesting that the Mn-Mn coupling is appreciably affected by Tb 4*f* electrons. In particular, due to the geometric location of Tb atoms (*i.e.* in between *ac*-planes), the main differences induced by the treatment of Tb 4*f* states occur in the out-of-plane interactions, appreciably affected by the 4*f* “spin-polarized” or “paramagnetic” electronic cloud in the (7↑,1↓) and (4↑,4↓) case, respectively.

At this point, one might infer that the stability of the AFM-E is closely related to

distortions (larger in HoMnO_3 , YMnO_3 and TbMnO_3 compared to LaMnO_3). Indeed, this is confirmed by our “artificial” structures: in $[\text{YMnO}_3]_{La}$ the reduced distortions - compared to YMnO_3 in equilibrium - restore the stability of the AFM-A (similar to LaMnO_3), whereas the increased distortions in $[\text{LaMnO}_3]_Y$ - compared to LaMnO_3 at equilibrium - make the AFM-E the ground state. Therefore, the stability of the AFM-E seems to be mainly connected with *structural* (*i.e.* octahedral distortions) more than with *chemical* (*i.e.* identity of the rare-earth element) effects.

In order to investigate the role of electronic correlation on the stability of the different magnetic states, we performed some calculations for YMnO_3 in the FM, AFM-A and AFM-E, according to an LSDA+U (or GGA+U) approach in the “atomic-limit”¹³ and varying the U value from 0 to 8 eV, keeping the U/J ratio fixed and choosing $J=0.15*U$. In Fig.2 a) we show the difference between total energies in the AFM-A and FM as well as in the AFM-E and FM. For a complete description of the electronic and magnetic structure, we also report the variation of the magnetic moment and of the band-gap as a function of the Coulomb parameter (see Fig. 2 b) and c), respectively). The bandgap and the magnetic moment both increase as a function of U, with a strong and rather weak dependence on the Coulomb parameter, respectively. This is expected, since LSDA+U tends to enhance the “localization” of Mn *d* states (thereby increasing the magnetic moment) and to push unoccupied states up in energy (thereby increasing the band-gap). As far as the magnetic ground state is concerned, our results show that the stability of the AFM-E and AFM-A is strongly affected by correlation effects: for values of U larger than 4 (7.5) eV, the FM is stabilized with respect to the AFM-E (AFM-A). We remark that the LSDA+U formalism might overestimate the tendency towards ferromagnetism, as already noted by Terakura and coworkers for LaMnO_3 ²¹ and consistently with our results in YMnO_3 . In addition, to our knowledge and at present, there are no spectroscopic works for YMnO_3 in the orthorhombic phase, on the basis of which one could extract the value of the Coulomb parameter. So, the LSDA+U results are mainly shown to warn the reader that the magnetic ground state may be affected by correlation effects. We hope our work will stimulate further experimental works on distorted manganites to gain additional insights on the accuracy of bare GGA vs GGA+U in treating these systems.

More information on the magnetic interactions between Mn atoms can be gained by considering a Heisenberg Hamiltonian²⁰ and using this model to fit our GGA-calculated

total energies. In particular, we consider the first- nearest-neighbor (J_{\parallel}^{nn}) and second nearest-neighbor coupling (J_{\parallel}^{nnn}) in the ac plane, as well as the first- and second-nearest-neighbour coupling out-of-plane (J_{\perp}^1 and J_{\perp}^2). Before discussing quantitatively our results, let us first recall what happens in the well-understood LaMnO_3 , showing a smaller GdFeO_3 -type distortion: the nn FM superexchange (SE) between e_g spins competes with the AFM SE between t_{2g} spins.¹⁸ The delicate balance of these two mechanisms crucially depends on the MnO_6 tilting and Jahn-Teller distortions.¹⁵ Indeed, this is evidenced by our results: for the heavily distorted compounds, the FM nn exchange parameters ($J_{\parallel}^{nn} \sim -1-2$ meV) are smaller in module⁹ than the much larger value in LaMnO_3 ($J_{\parallel}^{nn} \sim -9$ meV). This can be explained considering that, upon large tilting (*i.e.* in HoMnO_3 , TbMnO_3 and YMnO_3), the overlap between Mn $3d$ and O $2p$ orbitals is not large enough to provide a strongly FM SE between Mn cations in the ac plane. In turn, this alters the delicate balance with the nnn SE interactions through Mn-O-O-Mn paths along the a direction. Upon significant GdFeO_3 -distortions, the large J_{\parallel}^{nnn} (of the order of few meV in all compounds) AFM coupling prevails, therefore stabilizing the AFM-E ordering. Furthermore, the out-of-plane coupling between t_{2g} spins (J_{\perp}^1 of the order of few meV) keeps a strong AFM character along the R series, whereas we obtain very small (< 0.5 meV) J_{\perp}^2 coupling perpendicular out-of-plane. Finally, the octahedral distortions also affect this interplanar coupling (J_{\perp}^1 is smaller in LaMnO_3 than in distorted manganites), therefore weakening the assumption, very common in model hamiltonians, of restricting the study to a 2D square lattice^{8,9}, neglecting out-of-plane effects.

Let us now discuss the electronic and magnetic properties of the AFM-E phase, in terms of magnetic moments, band structures and density of states. The GGA Mn local magnetic moment ($\sim 3.3 \mu_B$) is reduced with respect to the Hund's rule value ($4\mu_B$), reflecting the hybridization with O atoms (slightly ferromagnetically polarized). The GGA-calculated total density of states and band-structure for the AFM-E YMnO_3 are reported in Fig. 3. Common to the well studied LaMnO_3 and shown by the density of states projected on the muffin-tin spheres (not reported), there is a strong hybridization between Mn d and O p states. In particular, the bands lying just below E_F (see highlighted states in Fig.3 (a) and (b)) and separated by the rest of the valence band are Mn-O bands (occupied hybridized e_g -like states). In agreement with the experimentally observed insulating character⁹, the resulting band structure shows an indirect band gap, with the conduction band minimum at

Γ and the valence band maximum at the Brillouin zone edge along the $[010]$ line and - more or less degenerately - along the $[110]$ - Γ line. It is interesting to note that, even without the introduction of the on-site Coulomb U repulsion, the AFM-E configuration shows an energy gap, in agreement with the experimental observation of an insulating behaviour. When comparing with the metallic character of the cubic perovskite-like systems (not shown), despite their FM or AFM spin alignments, the effect of the Jahn-Teller distortion and of the octahedral tilting is seen to result in a removal of states at the Fermi level by opening band gaps.¹⁷ As shown in Fig.2 c), the precise value of the band-gap is strongly affected by the inclusion of correlation effects: for the extreme case of $U = 8$ eV, the gap increases up to ~ 2.5 eV. Finally, in order to have some hints on the orbital physics in AFM-E, we plot in Fig. 3 (c) the YMnO_3 total charge density of the occupied e_g^\uparrow states (in the $[-0.7;0]$ eV energy range with respect to E_F), which remarkably shows the staggered ordering of the relevant e_g orbital occurring in the Mn basal plane.

IV. CONCLUSIONS

In summary, we have shown via density-functional-based methods that in manganites with highly distorted MnO_6 octahedra, such as HoMnO_3 , TbMnO_3 and YMnO_3 , the insulating AFM-E phase is stabilized. This is in excellent agreement with experiments, where the AFM-E is observed for HoMnO_3 . The calculated exchange parameters show that GdFeO_3 -like distortions - that increase along the rare-earth series - reduce the in-plane nearest-neighbor FM superexchange interaction along the Mn-O-Mn path. This interaction, along with the delicate interplay with the AFM next-nearest-neighbors superexchange along planar Mn-O-O-Mn paths is ultimately responsible for the stabilization of the peculiar AFM-E spin arrangement. Although the approximations made in this study (such as partially inaccurate treatment of correlation effects and atomic relaxations, etc.) should well be tested in the near future, we hope that these results will stimulate more works - both from theory and experiments - to ascertain the role played by the AFM-E magnetic configuration in the manganites framework.

¹ Y. Tokura, Rep. Prog. Phys. **69**, 797 (2006) and references therein.

- ² M. B. Salamon and M. Jaime, Rev. Mod. Phys. **73**, 583 (2001) and references therein.
- ³ T. Kimura, T. Goto, H. Shintani, K. Ishizaka, T. Arima and Y. Tokura, Nature **426**, 55 (2003).
- ⁴ M. Kenzelmann, A. B. Harris, S. Jonas, C. Broholm, J. Schefer, S. B. Kim, C. L. Zhang, S. W. Cheong, O. P. Vajk and J. W. Lynn, Phys. Rev. Lett **95**, 087206 (2005).
- ⁵ A. Munoz, M. T. Casais, J. A. Alonso, M. J. Martinez-Lope, J. L. Martinez, M. T. Fernandez-Diaz, Inorg. Chem. **40**, 1020 (2001).
- ⁶ J. A. Alonso, J. L. Garca-Munoz, M. T. Fernandez-Diaz, M. A. G. Aranda, M. J. Martinez-Lope, and M. T. Casais, Phys. Rev. Lett. **82**, 3871 (1999); J.L.Garcia-Munoz, J. Rodriguez-Carvajal, P. Lacorre, Phys. Rev. B **50**, 978 (1994).
- ⁷ E.O. Wollan and W. C. Koehler, Phys. Rev. **100**, 545 (1955).
- ⁸ T. Hotta, M. Moraghebi, A. Feiguin, A. Moreo, S. Yunoki and E. Dagotto, Phys. Rev. Lett. **90**, 247203 (2003).
- ⁹ T. Kimura, S. Ishihara, T. Arima, K.T.Takahashi, K. Ishizaka and Y. Tokura, Phys. Rev. B **68**, 060403 (2003).
- ¹⁰ E. Wimmer, H. Krakauer, M. Weinert and A. J. Freeman, Phys. Rev.B **24**, 864 (1981).
- ¹¹ <http://www.flapw.de>
- ¹² L. Nordstroem and A. Mavromaras, Europhys. Lett. **49** 775 (2000); M. Divis, K. Schwarz and P. Blaha, G. Hilscher and H. Michor, and S. Khmelevskiy, Phys. Rev. B **62**, 6774 (2000).
- ¹³ V. Anisimov, F. Aryasetiawan, and A. I. Liechtenstein, J.Phys.: Condens. Matter **9**, 767 (1997).
- ¹⁴ A. Shick, A. I. Liechtenstein, W. E. Pickett, Phys. Rev. B **60**, 10763 (1999).
- ¹⁵ J. A. Alonso, M. J. Martinez-Lope, M.T. Casais, M. T. Fernandez-Diaz, Inorg. Chem. **39**, 917 (2000).
- ¹⁶ T. Mizokawa, D. I. Khomskii and G. A. Sawatzky, Phys. Rev. B **60**, 7309 (1999).
- ¹⁷ P. Ravindran A. Kjekshus, H. Fjellvag, A. Delin and O.Eriksson, Phys. Rev. B **65**, 064445 (2002).
- ¹⁸ N. Hamada, H. Sawada, and K. Terakura, in *Spectroscopy of Mott Insulators and Correlated metals*, eds. A. Fujimori and Y. Tokura (Springer, Berlin, 1995); H. Sawada, Y. Morikawa, K. Terakura and N. Hamada, Phys. Rev. B **56**, 12154 (1997).
- ¹⁹ Incidentally, we note that our results for LaMnO₃ are in overall good agreement with previous first-principles calculations, such as Refs.^{17,21}.
- ²⁰ Model-hamiltonians for manganites generally include an orbital-ordering term in addition to

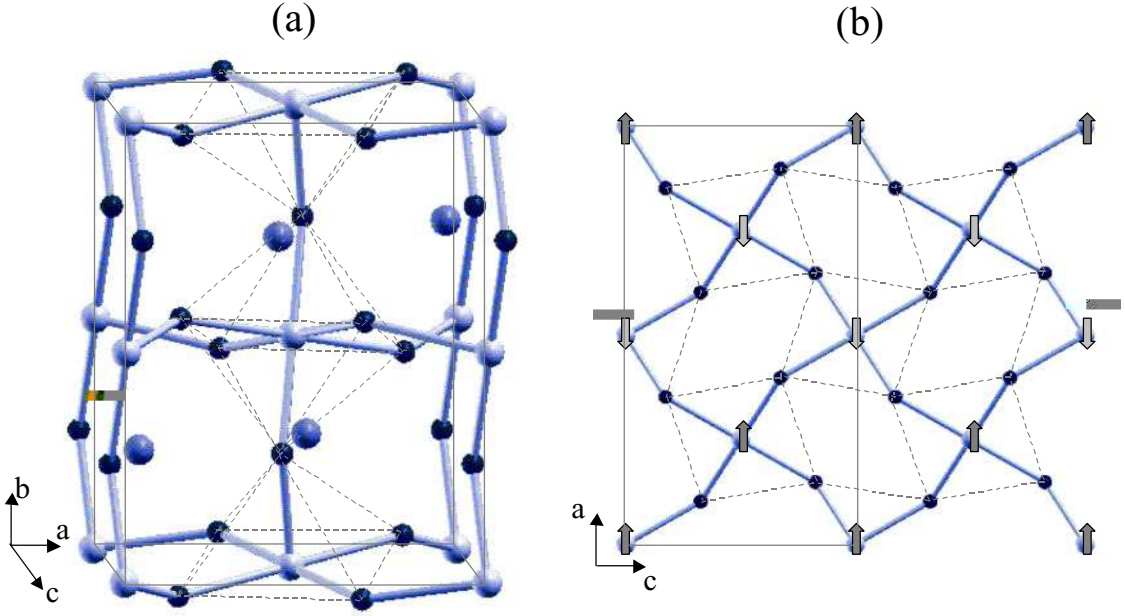


Fig. 1 - Picozzi et al.

FIG. 1: (Color online) (a) The $Pnma$ orthorhombic cell of $RMnO_3$. Black, white and grey spheres represent O, Mn and Tb (or Y or La or Ho) atoms, respectively. (b) ac in-plane view of MnO_2 planes, showing the large octahedral distortions and “up-up-down-down” zig-zag spin ordering. Solid lines mark the in-plane projected unit-cell.

spin-spin coupling, which, however, goes beyond the scope of the present work.

²¹ I. Solovyev, N. Hamada and K. Terakura, Phys. Rev. B **53**, 7158 (1996).

TABLE I: Calculated total energy difference (in meV/Mn) with respect to the FM phase. Recall that *i*) type-E consists of intraplane up-up-down-down and interplane AFM coupling; *ii*) type-E* consists of intraplane up-up-down-down and interplane FM coupling; *iii*) type-A consists of interplane AFM and intraplane FM coupling; *iv*) type-C consists of intraplane AFM and interplane FM coupling; *v*) type-G consists of both interplane and intraplane AFM coupling. Numbers in bold denote the ground state.

	YMnO ₃	HoMnO ₃	TbMnO ₃ ($7\uparrow, 1\downarrow$)	TbMnO ₃ ($4\uparrow, 4\downarrow$)	LaMnO ₃	[YMnO ₃] _{La}	[LaMnO ₃] _Y
FM	0	0	0	0	0	0	0
AFM-E	-44	-37	-32	-45	-2	+13	-61
AFM-E*	-23	-12	-11	-30	+2	+15	-34
AFM-A	-29	-16	-8	-21	-17	-7	-38
AFM-C	-10	-2	+17	+9	+58	+78	-33
AFM-G	-24	-14	+4	-17	+64	+88	-52

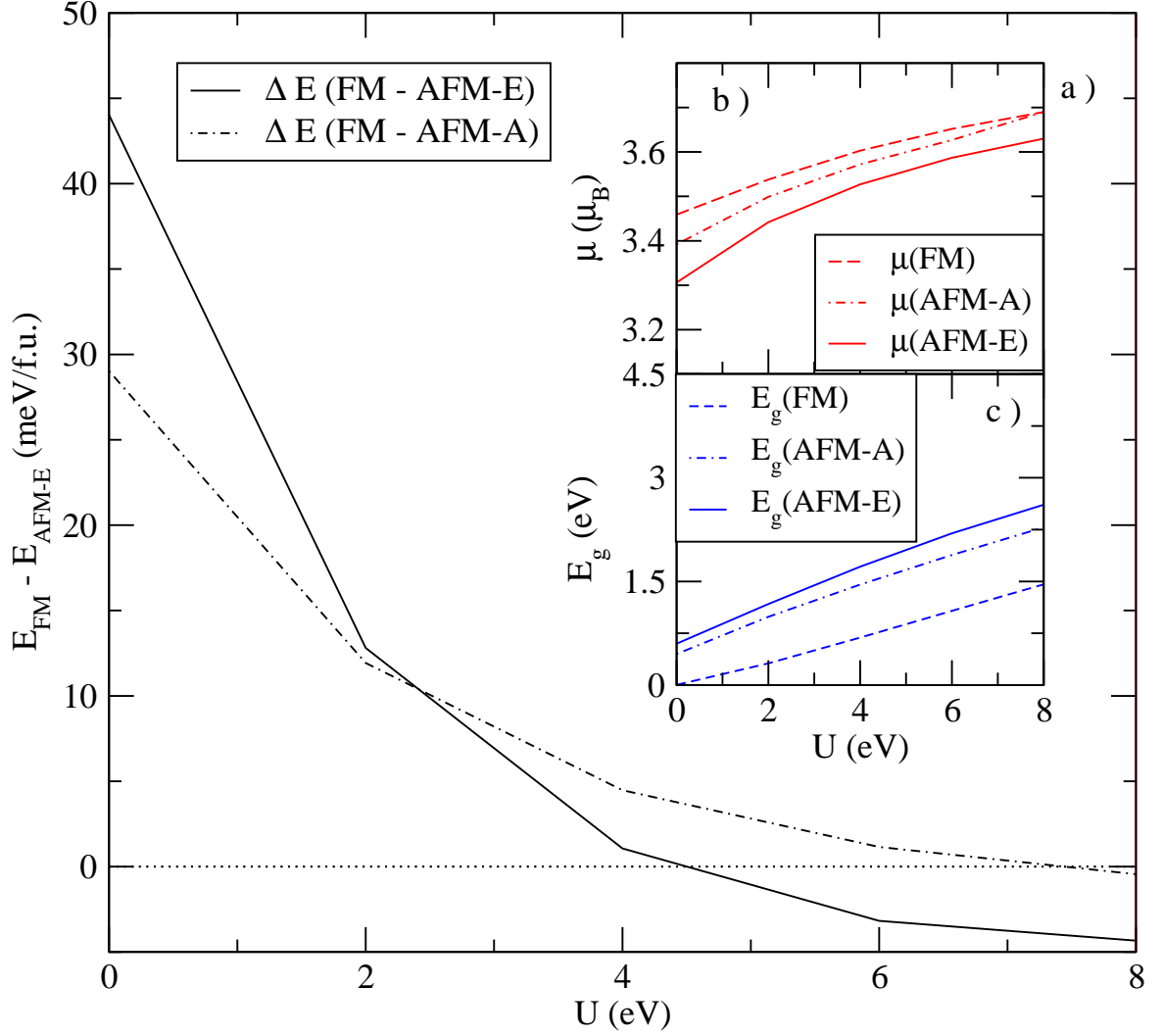


Fig. 2 - Picozzi et al.

FIG. 2: (Color online) (a) Difference (in meV/formula-unit) between the FM and AFM-E (black solid line) and the FM and AFM-A (black dot-dashed line) as a function of the Coulomb parameter for YMnO_3 . J is set to $0.15 \cdot U$. The changes of (b) Mn magnetic moment and (c) band-gap as a function of U are also shown for the different phases: FM (dashed line), AFM-A (dot-dashed line) and AFM-E (solid line).

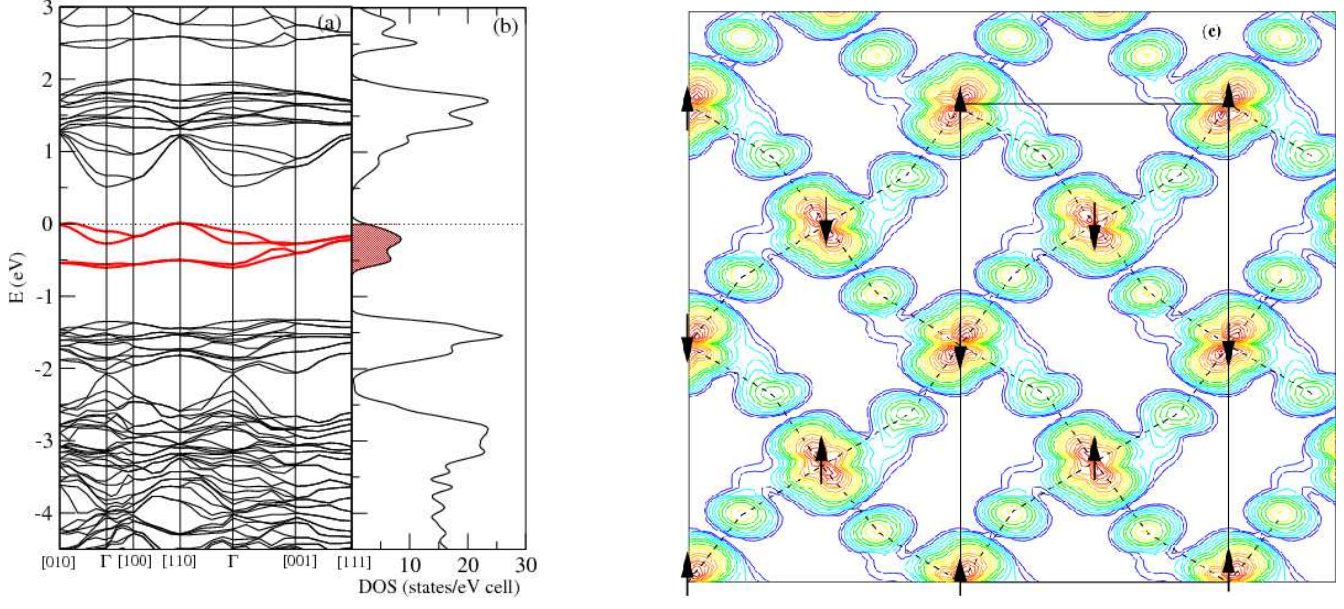


FIG. 3: (Color online) (a) Band-structure and (b) total DOS for YMnO₃ in the AFM-E magnetic configurations. (c) Total charge density contour plots for occupied e_g states. Arrows denote the Mn spins; the solid lines mark the unit cell.